Measurement of Pionium Lifetime

B. Adeva, A. Romero, O. Vázquez Doce

IGFAE, University of Santiago de Compostela, Spain

Abstract

We present in this note analysis results on $\pi^+\pi^-$ Coulomb interaction at very low Q using DIRAC Ni 2001 data. The enhancement observed at Q $\sim$ 1 MeV/c is shown to correspond to the production and subsequent break-up of pionium bound states, whose longitudinal and transverse spectra are fully mapped. Following the extrapolation method, independent measurements are made of pionium break-up probability in ten 600 MeV/c momentum bins, which lead to a measurement of pionium lifetime. The most significant contributions to systematic error are analysed.

DIRAC internal note 2006 *12 June 2006*

1 Data selection

The analysis presented in this note has used the standard pre-selection procedure described in http://dirac.web.cern.ch/DIRAC/pre-sel.html, for 2001 Ni target events. It is generally accepted that the cuts introduced in this filtering procedure do not produce any significant bias in the shape of two-pion Coulomb interaction spectrum, further than shrinking the Q_T distribution to an approximate cut of $Q_T < 6MeV/c$. In particular, they are sufficiently general not to introduce bias in upstream detector multiplicities. However, no specific attempt has been made on our side to cross-check this point so far.

The main use of this pre-selection stems from the strong data reduction, which facilitates data processing through multiple iterations. This is of course at the cost of having slightly reduced experimental constraints in the description of the Q_T spectrum of Coulomb interaction background. As we shall see, the Q_L spectrum will effectively provide such constraint.

2 Reconstruction method

Pions are reconstructed according to the method described and evaluated in [4], which is a switchable option of the standard ARIANE program (version 304-43 was used in present analysis). This method has the distinct feature of having independent tracking in the upstream and downstream arms. This becomes possible when the full upstream spectrometer information is used, consisting (in 2001) of 10 detector layers of MSGC/GEM, Scintillation Fibre Detector (SFD), and Ionisation Hodoscope (IH) [1]. In this region stray fields are negligible, so straightline fitting allows unambiguous reconstruction of pion pairs pointing to the beam intersection with the target. In a high radiation environment, this is important. The opening angle is then determined with very high precision (practically limited by multiple scattering inside the target foil only), therefore Q_T resolution is excellent. Charge confusion is inevitable at very low opening angles (due to limited angle resolution in DC track extrapolation through the dipole magnet), but the sign of Q_T is not an objective of the experiment, since charge-conjugation symmetry is taken for granted in pion-pion interaction.

Upstream tracks make use of stereo angles of 4 MSGC detectors, in conjuntion with TDC information from extrapolated X or Y SFD hits. As a consequence, they have a well defined time tag, which reduces the noise from out-of-time MSGC hits to a small amount.

As mentioned, upstream track pairs are matched with DC tracks in order to determine the correct charge assignment. Matching efficiency is uniform over detector acceptance, and it exceeds 95% everywhere [4] [5]. Time information is used as part of the matching procedure. Pulse-hight in IH is calibrated with single and double upstream tracks. Double ionisation signal is required in this detector to identify pion pairs, when only a single unresolved track can be matched to DC tracks.

In order to improve precision and minimize the effect of multiple scattering in the break-up probability measurement, only the signals from MSGC/GEM detector are used in the final track re-fit [5].

Standard cuts for muon background rejection using muon counters and pre-shower detector (PSH) are applied, and PSH pulses have been analysed to cross-check and improve Cherenkov veto efficiency.

3 Monte Carlo simulation

In order to achieve the most accurate extrapolation of Coulomb interaction down to very small values of Q, we have chosen Monte Carlo simulation as the simplest analysis procedure. In addition, 50 % of the experiment DAQ was designed to collect accidental pairs, which were used in this analysis to perform trigger acceptance corrections to Q_L spectrum.

In should be understood that the use of Monte Carlo is entirely restricted to the description of experimental resolution, and by no means it implies specific model assumptions about proton-nucleus physics. In particular, Coulomb interaction is described by the Gamow enhancement of their Q-space wave-functions. The effect of the η' and ω large-size resonances is taken into account separately as a small correction [6]. Even with the excellent time-of-flight resolution of the spectrometer, a non-Coulomb background remains in prompt-pair event selection. It consists of accidental pairs and other long-lifetime decays. Both are described by Monte Carlo, where pion pairs are simulated isotropically in their center-of-mass frame, and the Coulomb factor is removed [7].

The input lab-frame pion momentum spectrum p is actually taken from real spectrometer data. For this purpose, a de-convolution of the reconstructed prompt pair spectrum E as function of p and θ_b (angle with respect to the proton beam) is performed, according to the expression:

$$G_1(p,\theta_b) = \frac{E(p,\theta_b)}{\epsilon(p,\theta_b)} \frac{1}{A_C(Q)}$$

where $A_C(Q)$ is the Coulomb factor and the acceptance function ϵ is evaluated by Monte Carlo as follows :

$$\epsilon(p, \theta_b) = \frac{R(p, \theta_b)}{G_0(p, \theta_b)}$$

where R is the Monte Carlo reconstructed output for a given generator input G_0. The procedure was iterated only once, and G_1 taken as final generator input. The acceptance function matrix $\epsilon(p, \theta_b)$ does not appear to depend significantly on G_0. Two different G_1 functions were determined, one for prompt events and another for accidental pairs. The latter (obtained with $A_C(Q) = 1$), is used for simulation of the accidental pair background in prompt events. Their corresponding spectra $E(p, \theta_b)$ do differ significantly, mainly due to the proton background which is present in accidental pairs. In fact, this point has been verified following the procedure outlined in reference [8] for 2001 data.

GEANT tracking is performed by the GEANT-DIRAC program [2] with standard geometry and detector files, but with modified average multiple scattering angle according to reference [9]. GEANT detector digitisations were performed by ARIANE program [3]. The procedure for MSGC cluster patterning uses real data input to describe correlations between cluster total charge, micro-strip multiplicity and differential charge. Input data were selected to correspond to 2001 runs specifically.

Simulation of out-of-time noise hits in MSGC detectors is done by reproducing the experimentally observed characteristics of this background, namely:

- existence of significant hit multiplicity correlations from plane to plane (4 detectors), which are encoded by specific arrays determined from real data.
- absence of space correlations between different planes, once the two $\pi^+\pi^-$ triggering tracks are removed, thus indicating this background essentially originates from wide angle tracks with respect to the beam direction.

In figure 1 we compare the observed MSGC hit multiplicity distributions for each detector with Monte Carlo simulation. Only hits (real or background) found within a momentum-dependent $\pm 3\sigma$ space window from a drift chamber track are retained. As it can be appreciated, MSGC background is perfectly well described.

A delicate challenge to the DIRAC reconstruction procedure arises from the response of Peak Sensing Circuit (PSC) electronics of the scintillation fibre detector, when two pulses arrive in strict time coincidence (prompt pairs) and within a given 8-channel group. In this case, suppresion of one of the pulses occurs with a significant probability, at the level of 20-40% [1]. The distorsion caused by this effect in close-pair efficiency at small distances (below 3 mm) is

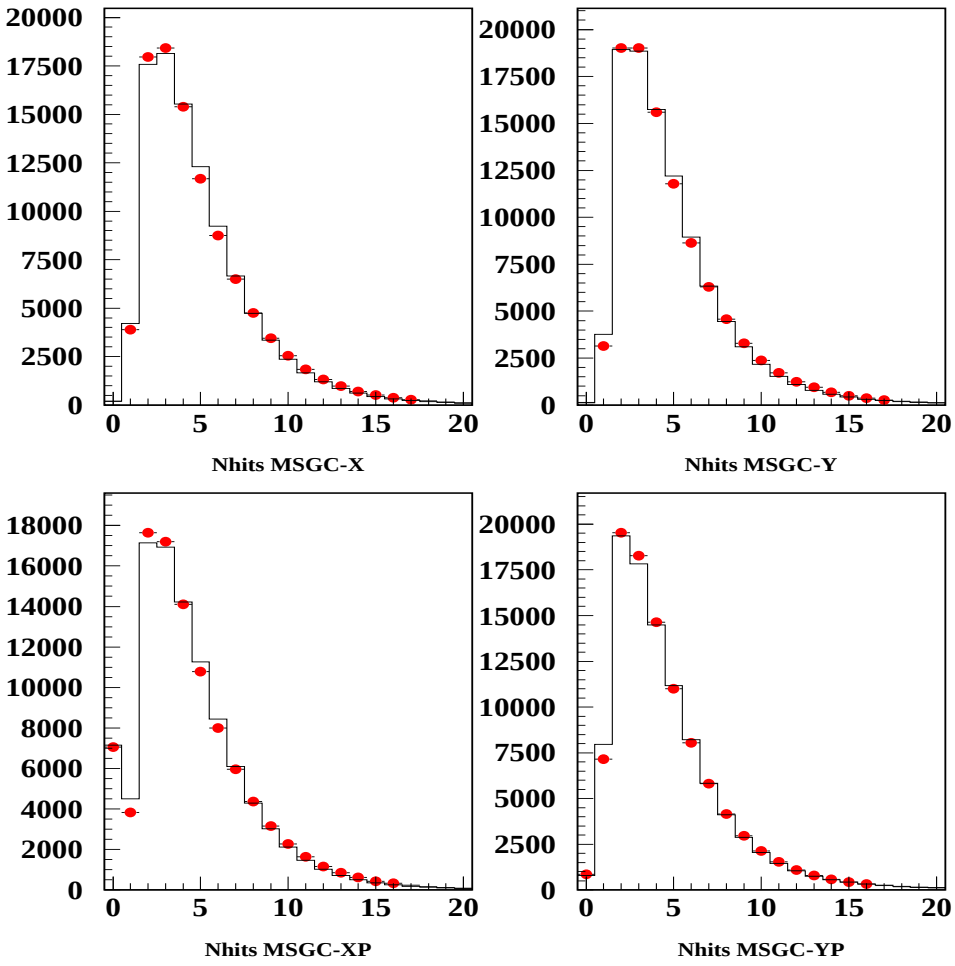

Fig. 1. *Number of MSGC clusters found close to any of the drift chamber tracks, including the real signal pairs (dots), compared to Monte Carlo simulation (line). Detector ordering is X/Y (top left/right) and X' / Y' (bottom left/right). All data runs used in lifetime analysis were included.*

largely diminished when the previously described upstream tracking is used, where only one SFD hit (in X or Y projection) is required to perform time tagging, the track being actually measured by MSGC hits having stereo angles.

4 Analysis of Q-spectrum

A two-dimensional analysis of $\pi^+\pi^-$ spectrum in the center-of-mass frame has been carried out, choosing the transverse $Q_T = \sqrt{Q_X^2 + Q_Y^2}$ and longitudinal $Q_L = |Q_Z|$ components (with respect to the pair direction of flight Z)

as independent variables. This analysis has been done independently at ten individual $600 MeV/c$ bins of the laboratory-frame momentum p (magnitude of 3-vector sum of pion momenta p_1 and p_2) , and also globally including all values of p in the same fit. The results will be presented in sections 6 and 7. Irrespective of the parameter variation strategy, or of the momentum definition followed in each case, the prompt two-pion spectrum in (Q_T, Q_L) plane has been χ^2-analysed by comparison with the following input spectra:

- Monte Carlo describing the Coulomb final-state interaction by means of the Sakharov-Gamow-Sommerfeld factor (labelled CC), using single pion lab-frame momentum from de-convoluted prompt spectrometer data.
- Monte Carlo describing accidental coincidences taken by the spectrometer (labelled AC). It represents the uncorrelated non-Coulomb background in prompt events. Its laboratory momentum spectrum has been generated according to that of true accidental pairs taken by the spectrometer, after de-convolution of detector acceptance. Its fraction has been determined from the time-of-flight (TOF) spectrum in each momentum bin, and the values obtained are given in table 1
- Monte Carlo describing Coulomb non-interacting $\pi^+\pi^-$ (labelled NC). It simulates accidental pairs as well as any additional fraction of non-Coulomb events where one of the pions originates from decay of long-lifetime resonances (up to ns scale). Such events are still detected as time-correlated by the precision coincidence of the spectrometer. We assume they have a strictly isotropical distribution in their center-of-mass frame. Their lab-frame momentum spectrum (entirely decoupled from Q-space) is also taken from spectrometer data.
- Pionium atom Monte Carlo model [7], which is used to cross-check and fit the observed deviation with respect to the continuum Coulomb background spectrum constructed from the previous input (it is labelled AA)

The total number of events used from the above samples are denoted by N_{CC},N_{AC},N_{NC} and N_{AA} respectively, whereas N_p represents the total number of prompt events in the analysis, under the reference cuts $Q_T < 5 MeV/c$ and $Q_L < 20 MeV/c$. Index k runs over all (i,j) bins of the (Q_T, Q_L) histograms, and we denote by N^k_{CC} the number of Coulomb events observed in each particular bin (i,j). Similarly for the other input spectra, namely N^k_{AC}, N^k_{NC} and N^k_{AA}. Normalised spectra are used to fit the data, and we denote them by small letters, $n^k_{CC} = N^k_{CC}/N_{CC}$ and likewise for the rest. The ratios $x_{CC} = N_{CC}/N_p$, $x_{AC} = N_{AC}/N_p$, $x_{NC} = N_{NC}/N_p$ and $x_{AA} = N_{AA}/N_p$ help define the statistical errors. The χ^2 analysis is based upon the expression:

$$\chi^2 = \sum_k \frac{\left(N^k_p - \beta\alpha_1 n^k_{CC} - \beta\alpha_2 n^k_{AC} - \beta\alpha_3 n^k_{NC} - \beta\gamma n^k_{AA}\right)^2}{\beta\left(n^k_p + n^k_{CC}(\frac{\alpha_1^2}{x_{CC}}) + n^k_{AC}(\frac{\alpha_2^2}{x_{AC}}) + n^k_{NC}(\frac{\alpha_3^2}{x_{NC}}) + n^k_{AA}(\frac{\gamma^2}{x_{AA}})\right)} \quad (1)$$

Table 1
Fraction of accidental pairs determined from TOF spectrum at individual lab-frame momentum bins with $Q_L < 20MeV/c$.

p interval (GeV/c)	α_2
2.6-3.2	0.0773 ± 0.0002
3.2-3.8	0.0876 ± 0.0001
3.8-4.4	0.1038 ± 0.0001
4.4-5.	0.1139 ± 0.0001
5.-5.6	0.1203 ± 0.0002
5.6-6.2	0.1269 ± 0.0002
6.2-6.8	0.1348 ± 0.0003
6.8-7.4	0.1440 ± 0.0004
7.4-8.	0.1531 ± 0.0008
8.-8.6	0.1602 ± 0.0018

where α_i and γ are the respective Monte Carlo type fractions (according to $\alpha_1 + \alpha_2 + \alpha_3 + \gamma = 1$). A control region is defined by the cut $Q_L > 2MeV/c$, where we do not expect deviations with respect to the continuum Coulomb interaction background. We call $Q_L < 2MeV/c$ the extrapolation region.

Subtraction of accidental pairs is performed by blocking the α_2 parameter to the experimentally observed values. Minimisation of the above χ^2 over the entire (Q_T, Q_L) plane determines the non-Coulomb fraction α_3, and the atom fraction γ as free parameters. The β parameter, which represents the overall Monte Carlo normalisation, is actually determined by the number of prompt events in the domain under fit, and it does not need to be varied.

Once the previous fit has converged, we define the atom signal in each (i, j) bin as the difference between the prompt spectrum (after subtraction of accidentals) and the Monte Carlo with the pionium component (AA) removed. This 2D signal, which reveals the excess with respect to the calculated Coulomb interaction enhancement, is analysed in detail in sections 6 and 7, where it is compared with the Monte Carlo prediction for atom production. Further χ^2 tests are performed both in the $Q_L > 2MeV/c$ (control region, where pionium Monte Carlo does not contribute) and in the $Q_L < 2MeV/c$ (extrapolation region) separately.

Table 2
Numerical values of K^{th} and K^{exp} as defined in the text. Each raw corresponds to a given rectangular cut in (Q_T, Q_L) plane , with $Q_T^c = 5MeV/c$ and $Q_L^c = 20MeV/c$ being the reference cut values. K^{th} values are obtained by integration of (2) in cylindrical coordinates.

$Q_L^{cut}(MeV/c)$	K^{theo}	K^{exp}
0.5	0.4372	0.3017 ± 0.0010
1.0	0.2389	0.2193 ± 0.0005
1.5	0.1669	0.1618 ± 0.0003
2.0	0.1300	0.1274 ± 0.0002
$Q_T^{cut}(MeV/c)$	K^{theo}	K^{exp}
0.5	3.2457	0.8457 ± 0.0083
1.0	1.2382	0.6681 ± 0.0038
1.5	0.6995	0.5206 ± 0.0021
2.0	0.4674	0.4027 ± 0.0013
2.5	0.3426	0.3137 ± 0.0009
3.0	0.2660	0.2505 ± 0.0006
3.5	0.2147	0.2054 ± 0.0005
4.0	0.1781	0.1720 ± 0.0004
4.5	0.1509	0.1468 ± 0.0003
5.0	0.1300	0.1274 ± 0.0002

5 K-factors and break-up probability

The conversion from integrated atom production signal to break-up probability is done by means of the so-called K-factors, which are defined as follows.

Let us call $S_B(\Omega)$ the measured ratio between the number of atoms N_A and the number of Coulomb pairs N_C, both observed in the same kinematical region Ω of the (Q_T, Q_L) plane. This quantity can be converted into a measurement of the atom break-up probability P_{Br}, because the number of atoms n_A produced in a given phase-space volume can be calculated analytically in quantum mechanics [12] according to :

$$K^{th} = \frac{n_A}{N_C} = 8\pi^2 Q_0^2 \frac{\sum_1^\infty \frac{1}{n^3}}{\int A_C(Q) d^3Q} \qquad (2)$$

where the integral in the denominator extends over the desired Q-space volume. $Q_0 = \alpha M_\pi$ is two times the atom Bohr momentum p_B, and n its principal quantum number. For the sphere of radius $Q < Q_c$ the following expression is obtained:

$$K^{th}(Q_c) = \frac{n_A}{N_C} = \frac{\sum_1^\infty \frac{1}{n^3}}{\int_0^{Q_c/2p_B} \frac{kdk}{1-exp(-2\pi/k)}}$$

For a rectangular domain Ω in the (Q_T, Q_L) plane, integration of (2) in cylindrical coordinates provides the values given in table 2.

However, the actual K-factor which must be taken into account in the measurement (K^{exp}) differs from K^{th} due to experimental resolution [11] [**?**] , which is a function of domain Ω. The break-up probability is then determined as:

$$P_{Br} = \frac{S_B(\Omega)}{K^{exp}(\Omega)}$$

with the experimental K-factor defined in the following way:

$$K^{exp}(\Omega) = K^{th}(\Omega)\frac{\epsilon_A(\Omega)}{\epsilon_C(\Omega)}$$

where:

$$\epsilon_A(\Omega) = \frac{n_A^{rec}(\Omega)}{n_A^{gen}(\Omega)} \qquad \text{and} \qquad \epsilon_C(\Omega) = \frac{n_C^{rec}(\Omega)}{n_C^{gen}(\Omega)}$$

define the acceptance of the experimental apparatus as a whole for atoms and Coulomb pairs, respectively, in a given kinematical region Ω. The factors ϵ_A and ϵ_C are determined with high precision using separate Monte Carlo inputs, after processing the full simulation/digitisation/reconstruction chain. They are ratios between reconstructed output and generated input.

For a given momentum interval, the measured values of P_{Br} should not depend on the actual domain Ω which is chosen to perform the measurement, and this particular point will be studied in the following sections.

The K-factor values do however exhibit a momentum dependence, which we have analysed in detail, and it is indicated in table 3. These values have been taken into account in the determination of break-up probability in the next section.

Table 3
K-factors determined in 10 intervals of laboratory-frame momentum.

p interval (GeV/c)	$K-factor$
2.6-3.2	0.1140 ± 0.0005
3.2-3.8	0.1196 ± 0.0004
3.8-4.4	0.1267 ± 0.0005
4.4-5.	0.1316 ± 0.0005
5.-5.6	0.1368 ± 0.0007
5.6-6.2	0.1407 ± 0.0008
6.2-6.8	0.1431 ± 0.0011
6.8-7.4	0.1474 ± 0.0015
7.4-8.	0.1451 ± 0.0021
8.-8.6	0.1490 ± 0.0043

6 Use of accidental pairs and detector alignment for Q_L spectrum

Accidental pairs have been used to calibrate the spectrometer acceptance as function of Q_L, due to non-uniform trigger efficiency. The ratio R between Monte Carlo simulated non-Coulomb Q_L spectrum and that obtained from accidental pairs has been observed to be slightly non uniform. Since accidental triggers have undergone the same electronics readout chain as the prompt data, this ratio has been used as a correction factor to the Monte Carlo, in the analysis of Q_L spectrum. As it will be seen below, this is supported by the fact that the corrected results are in very good agreement with the analytical prediction based on the Sakharov factor for Coulomb pairs. This ratio R has been determined not only globally but also in each individual momentum interval. The correction has been smoothed by making linear or polynomial fits in the region $|Q_L| > 10MeV/c$, with results indicated in figure 2.

A precision analysis of Q_L spectrum further requires alignment of DC coordinates with respect to upstream detectors in the bending (X) projection, separately for positive and negative arms. This is achieved by ensuring that the Q_L distributions are accurately centered at zero in each momentum interval. Small shifts are observed with respect to the original calibration, which was based upon momentum-averaged deviations. As an illustration of the quality of the calibrated data, the asymmetry values around zero $A = (F-B)/(F+B)$

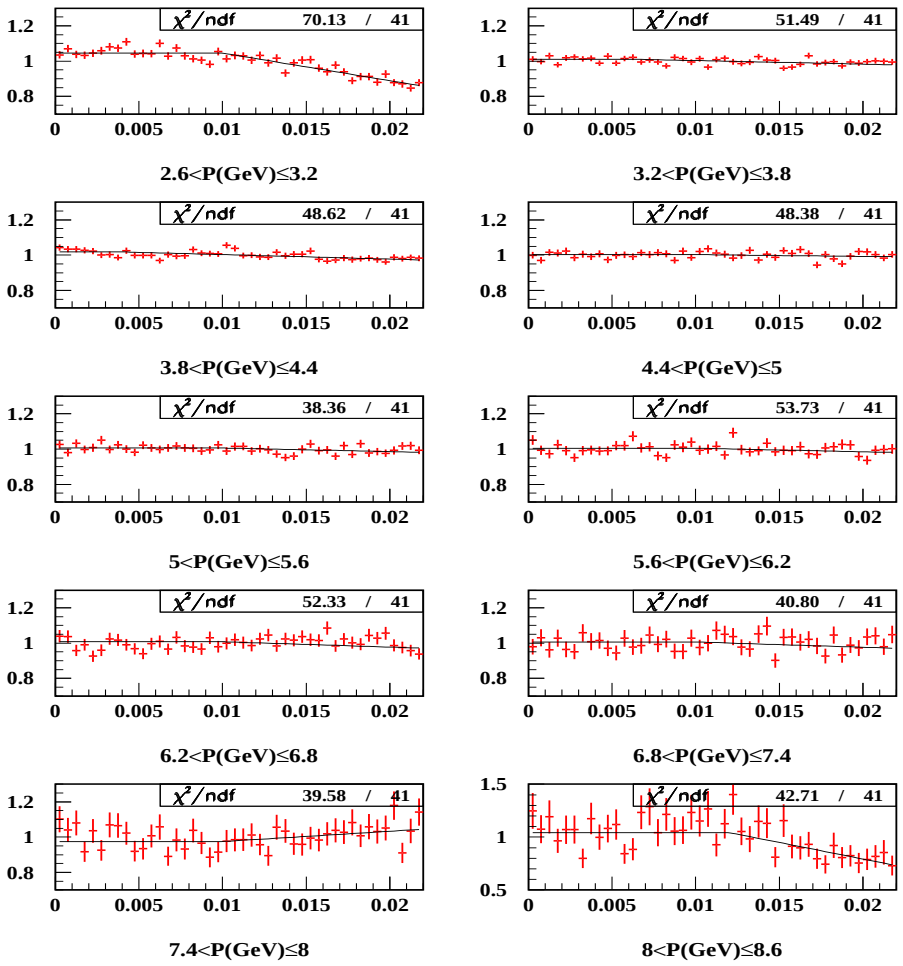

Fig. 2. *Ratio between non-Coulomb Monte Carlo and observed accidental Q_L spectrum in 10 different intervals of lab-frame momentum p*

are given in table 4 at every momentum bin (where $F = \int_{-X}^{0}(d\sigma/dQ_L)dQ_L$ and $B = \int_{0}^{X}(d\sigma/dQ_L)dQ_L$ with $X = 2MeV/c$).

7 Momentum-dependent fit results

Minimisation of χ^2 in expression (1) was carried out in $(0.5 \times 0.5)(MeV/c)^2$ bins of (Q_T, Q_L) space, independently in each of the ten 600 MeV/c lab-frame $\pi^+\pi^-$ momentum bins indicated in table 3, leaving α_1 and γ as free parameters. The α_2 parameter (fraction of accidental pairs) was blocked to the values experimentally observed from TOF, which were indicated in table

Table 4
Q_L asymmetry values around zero within $\pm 2 MeV/c$, after calibration at each momentum bin.

p interval (GeV/c)	asymmetry (error)
2.6-3.2	0.0058 ± 0.0066
3.2-3.8	-0.00005 ± 0.0053
3.8-4.4	0.0056 ± 0.0057
4.4-5.0	0.000017 ± 0.0065
5.0-5.6	-0.0013 ± 0.0076
5.6-6.2	-0.0043 ± 0.0091
6.2-6.8	0.0018 ± 0.0119
6.8-7.4	0. ± 0.0165
7.4-8.0	-0.0021 ± 0.0230
8.0-8.6	0.0201 ± 0.0344

1. The $\alpha_3 = 1 - \alpha_1 - \alpha_2 - \gamma$ fraction then measures the long-lifetime non-Coulomb component.

The fit quality is indicated by the χ^2-values obtained in each momentum bin, which are given in table 5. Although the pionium atom Monte Carlo has been used to guide the fit, the restriction of the χ^2 to the domain $Q_L > 2 MeV/c$ (where their contribution is very small) is equally good when the γ component is suppressed.

The extrapolation method can thus be applied to the region $Q_L < 2 MeV/c$, in such a way that an atom signal is defined in each (i, j) bin of (Q_T, Q_L) space by the difference between the prompt spectrum (accidentals subtracted) and the Monte Carlo prediction with pionium component removed.

The atom spectra are shown in figures 8 to 16 as function of Q_T and Q_L, and compared to the pionium Monte Carlo prediction in each case. The estimator of fit quality is provided by the χ^2 value extended over the extrapolation domain $(0, Q_T^c) \times (0, Q_L^c)$ with $Q_T^c = 5 MeV/c$ and $Q_L^c = 2 MeV/c$, with one degree of freedom used by the γ parameter. Those are given in last column of table 5. When the fit procedure is applied to the control region $Q_L > 2 MeV/c$, small deviations are still observed in Q_T spectrum, despite the acceptable values of χ^2. We attribute those to a remaining imperfection of the simulation of double-track resolution, and we actually improve the extrapolated spectrum by correcting for those deviations (observed in the control region) and pro-

jecting them them onto individual Q_T bins at $Q_L < 2MeV/c$. One degree of freedom is subtracted for every corrected Q_T bin.

The Q_L projection also requires a small acceptance correction, which is determined from accidental pairs, as it was described in section 6.

The number of atom pairs N_A determined as function of p is plotted in figure 4 along with the number of Coulomb pairs given by the fit in each case. Errors in N_A are given by MINOS variation of γ parameter. It is seen that atom production follows rather closely the spectrum of semi-inclusive $\pi^+\pi^-$ differential cross-section, as expected from bound state production. Please note that both of these spectra are uncorrected for spectrometer acceptance.

Pionium break-up probabilities can now be determined by using the momentum-dependent K-factors calculated in table 3, and they are shown in figure 3. Errors were propagated from those provided by the fit for N_A and N_C. P_{Br} values are compatible with a smooth increase with increasing atom momentum, as predicted by Monte Carlo tracking inside the target foil [7] [10]. The $1s$ pionium lifetime (τ_{1s}) can then be determined by χ^2 minimization with respect to the latter prediction, having τ_{1s} as only free parameter. Alternatively, P_{Br} measurements can be combined with independent statistical errors, and Monte Carlo tracking applied with a given atom momentum spectrum.

We have tested the stability of the measured values of P_{Br} at each momentum bin with respect to the upper limit Q_L^c chosen for the fit ($Q_L < Q_L^c$), which is shown in figure 22. Note that these results reveal good performance of the corrections shown in figure 2, based on the accidental spectrum.

The fitted values of α_1 parameter (fraction of Coulomb pairs) are also shown in figure 5 as function of p. They show little variation, compatible with a small linear increase.

In figure 6 we plot the remaining number of non-Coulomb pairs determined by the fit as function of p, after subtraction of accidentals according to table 1, and we compare the spectrum with that previously determined for Coulomb pairs (see figure 4). We attribute this reminder to a long-lived component in $\pi\pi$ prompt triggers, in a much shorter timescale than the TOF detector can appreciate ($\sim 170ps$). Although we have not attempted a detailed comparison with Monte Carlo models (with specific resonances), the observed softer spectrum is qualitatively well understood.

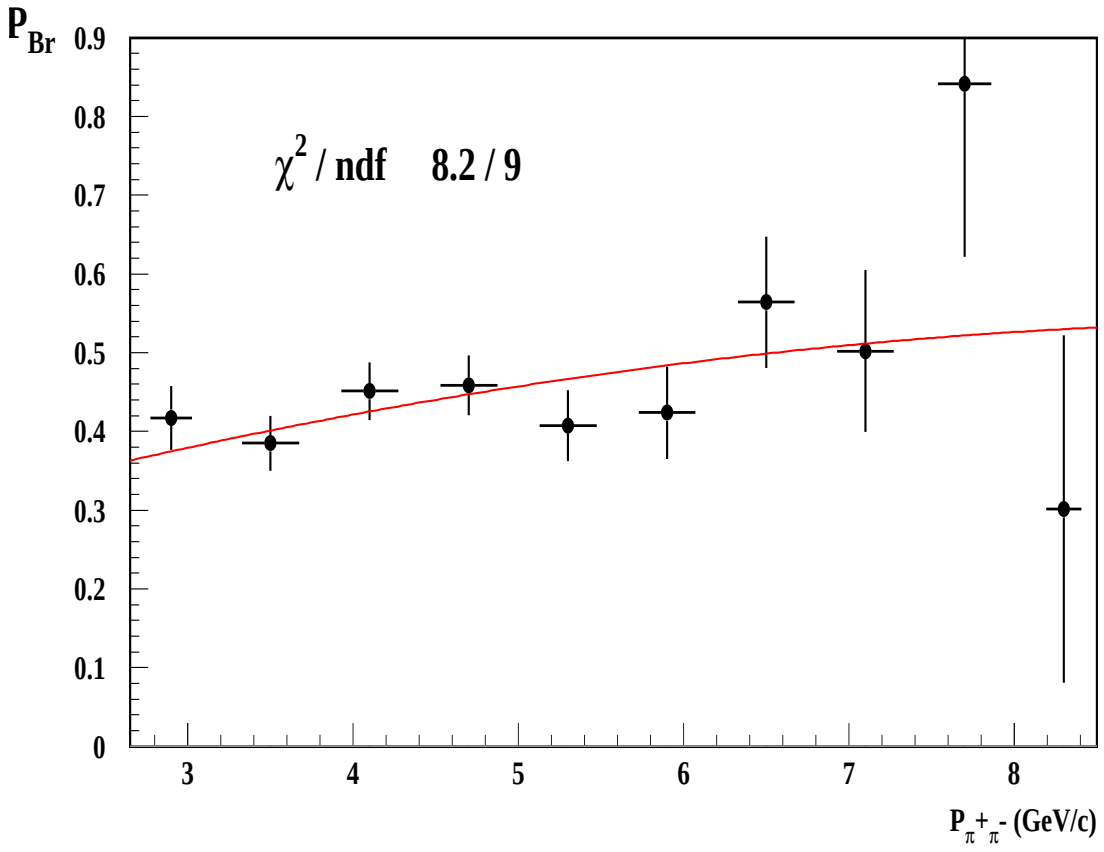

Fig. 3. *Pionium break-up probabilities as function of atom momentum, as compared to best fit Monte Carlo prediction with average Ni foil thickness.*

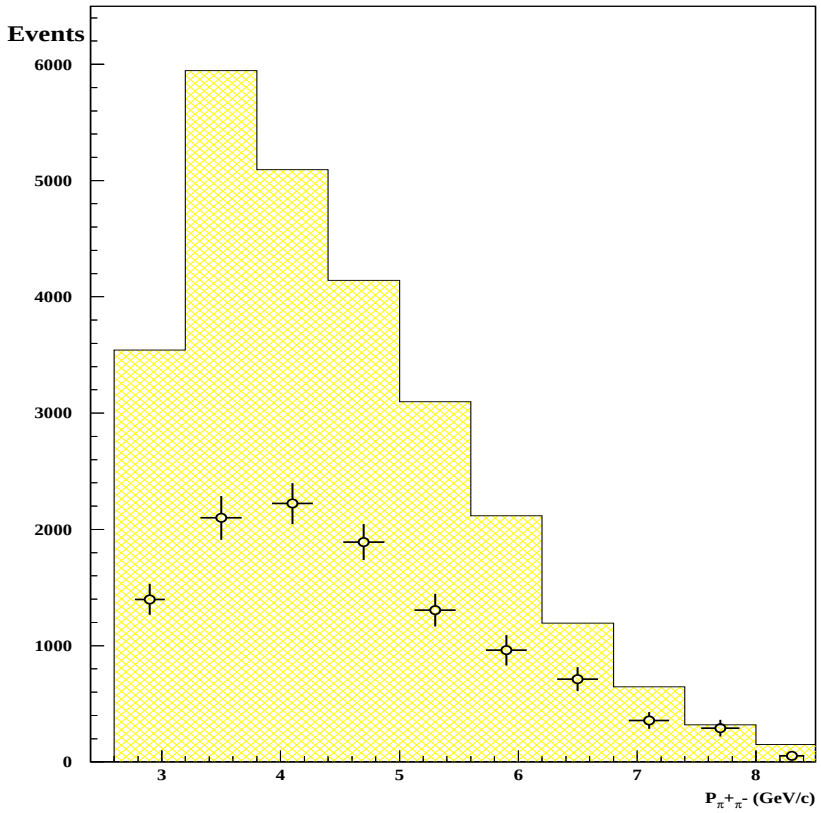

Fig. 4. *Fitted number of atom pairs as function of their lab-frame momentum (coloured) , as compared to the fitted number of Coulomb pais for* $Q_L > 2MeV/c$ *(black). The latter has been normalized to the same area, to avoid the large difference in actual scale.*

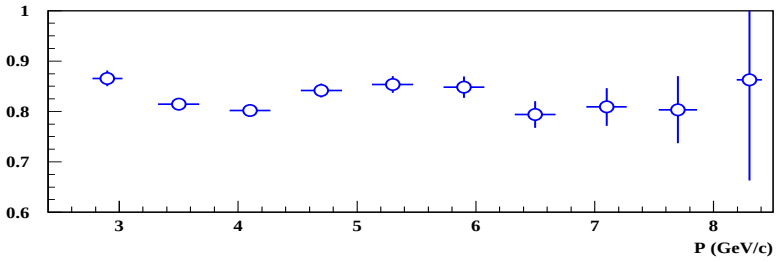

Fig. 5. *Fitted values of* α_1 *parameter as function of* $\pi^+\pi^-$ *momentum.*

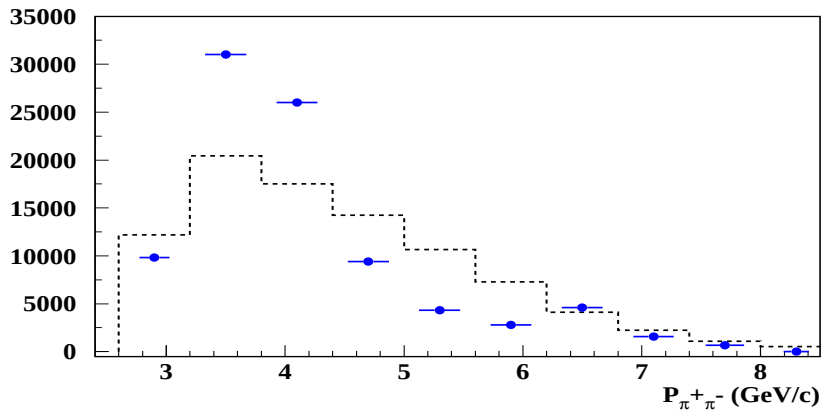

Fig. 6. *Fitted number of long-lifetime pairs (coloured), determined from α_3 parameter, as function of $\pi^+\pi^-$ momentum. It is compared with the number of Coulomb pairs shown in figure 4, normalized to the same area.*

Table 5
The main results of the fit concerning break-up probability P_{Br} , number of atom pairs N_A, α_1 and χ^2 over the entire fit region are indicated in this table, for every 600 MeV/c momentum interval p_i as defined in table 3.

	P_{Br}	N_A	α_1	χ^2 / ndf	χ^2_e / ndf
p_1	0.417 ± 0.041	839 ± 80	0.866 ± 0.016	320.6 / 350	45.8 / 40
p_2	0.385 ± 0.035	1260 ± 113	0.814 ± 0.011	360.9 / 350	45.7 / 40
p_3	0.451 ± 0.036	1333 ± 106	0.802 ± 0.012	355.1 / 350	25.5 / 40
p_4	0.459 ± 0.038	1135 ± 92	0.842 ± 0.014	337.3 / 350	30.5 / 40
p_5	0.407 ± 0.045	784 ± 85	0.853 ± 0.016	306.7 / 350	25.4 / 40
p_6	0.424 ± 0.058	577 ± 78	0.848 ± 0.021	335.1 / 350	46.8/ 40
p_7	0.564 ± 0.084	427 ± 62	0.794 ± 0.026	335.1 / 350	43.4 / 40
p_8	0.502 ± 0.103	214 ± 43	0.809 ± 0.037	333.3 / 350	66.8 / 40
p_9	0.841 ± 0.220	174 ± 43	0.804 ± 0.066	395.9 / 350	44.6 / 40
p_{10}	0.301 ± 0.220	32 ± 24	0.863 ± 0.000	344.1 / 350	54.1 / 40

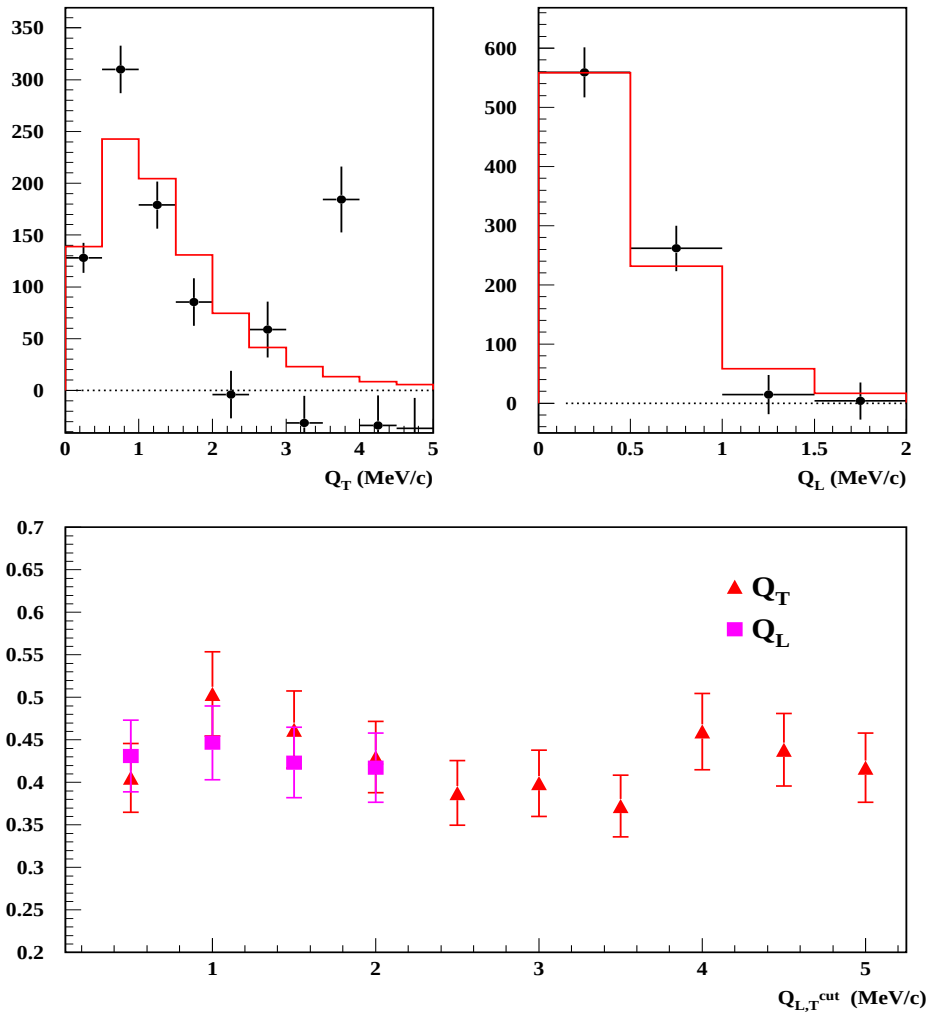

Fig. 7. *Fit results for a $\pi^+\pi^-$ momentum interval $2.6 < p < 3.2$ GeV/c in lab-frame. a) Transverse (Q_T) and longitudinal (Q_L) projections of the atom signal found in the extrapolation region ($Q_L < 2MeV/c$) after subtraction of the Monte Carlo prediction with pionium component removed (top). b) Differences in Q_L spectrum between the Monte Carlo prediction and the prompt data (center). c) Values of break-up probability determined for different integration upper limits (Q_T^u, Q_L^u) to define the atom signal (bottom).*

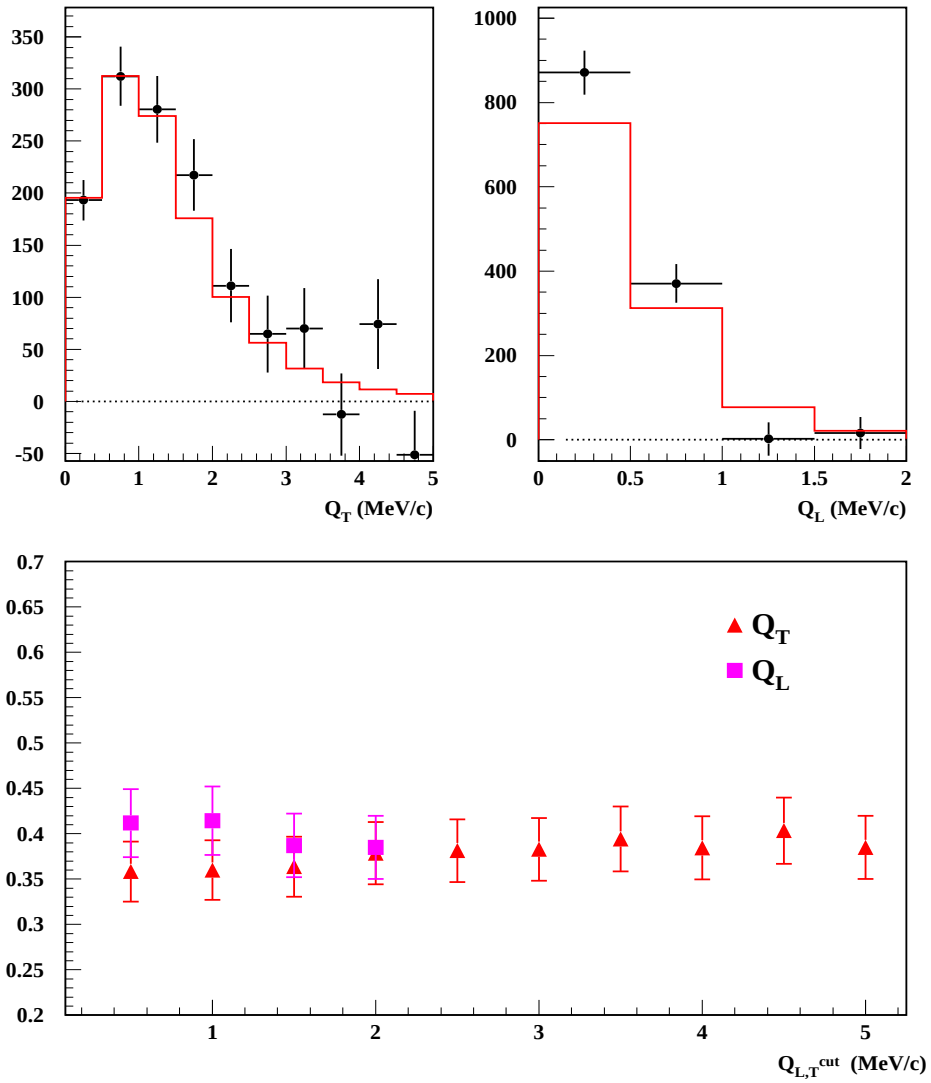

Fig. 8. *Fit results for a $\pi^+\pi^-$ momentum interval $3.2 < p < 3.8$ GeV/c in lab-frame. Caption is identical to figure 7.*

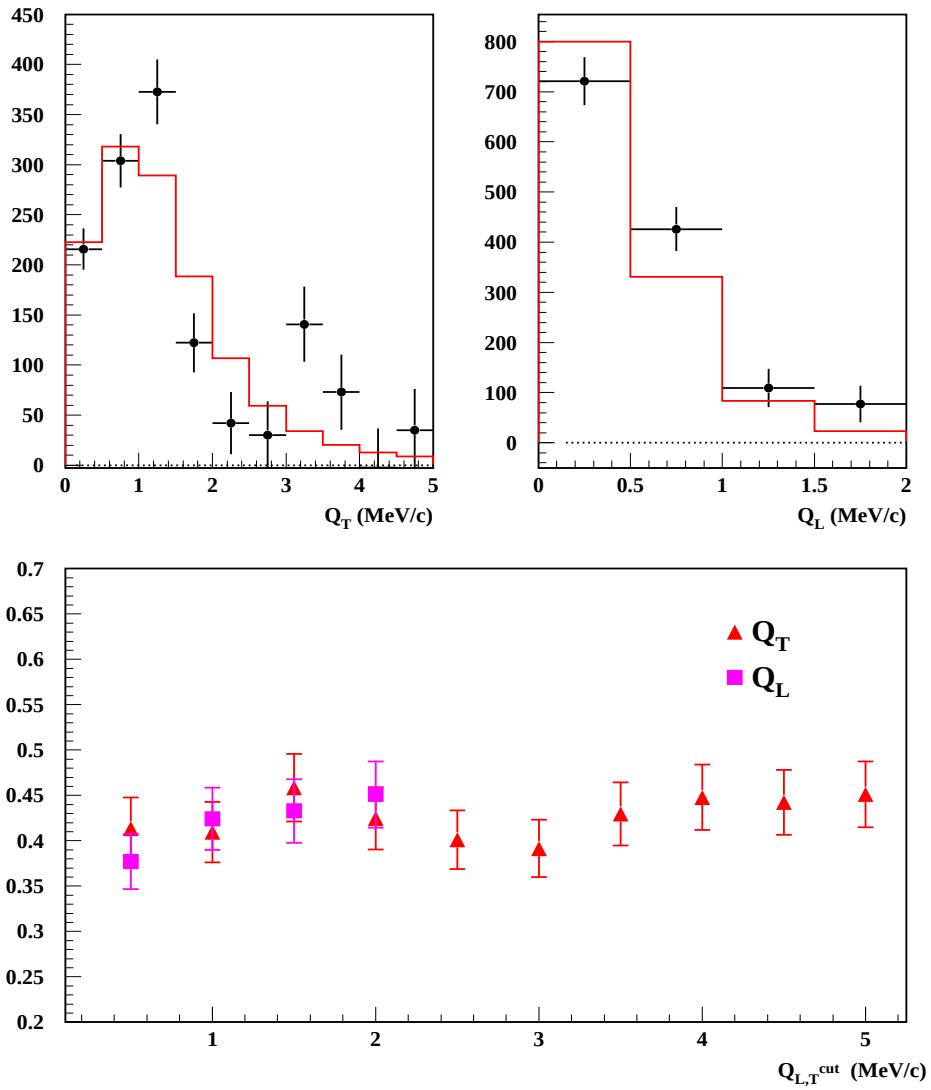

Fig. 9. *Fit results for a $\pi^+\pi^-$ momentum interval $3.8 < p < 4.4$ GeV/c in lab-frame. Caption is identical to figure 7.*

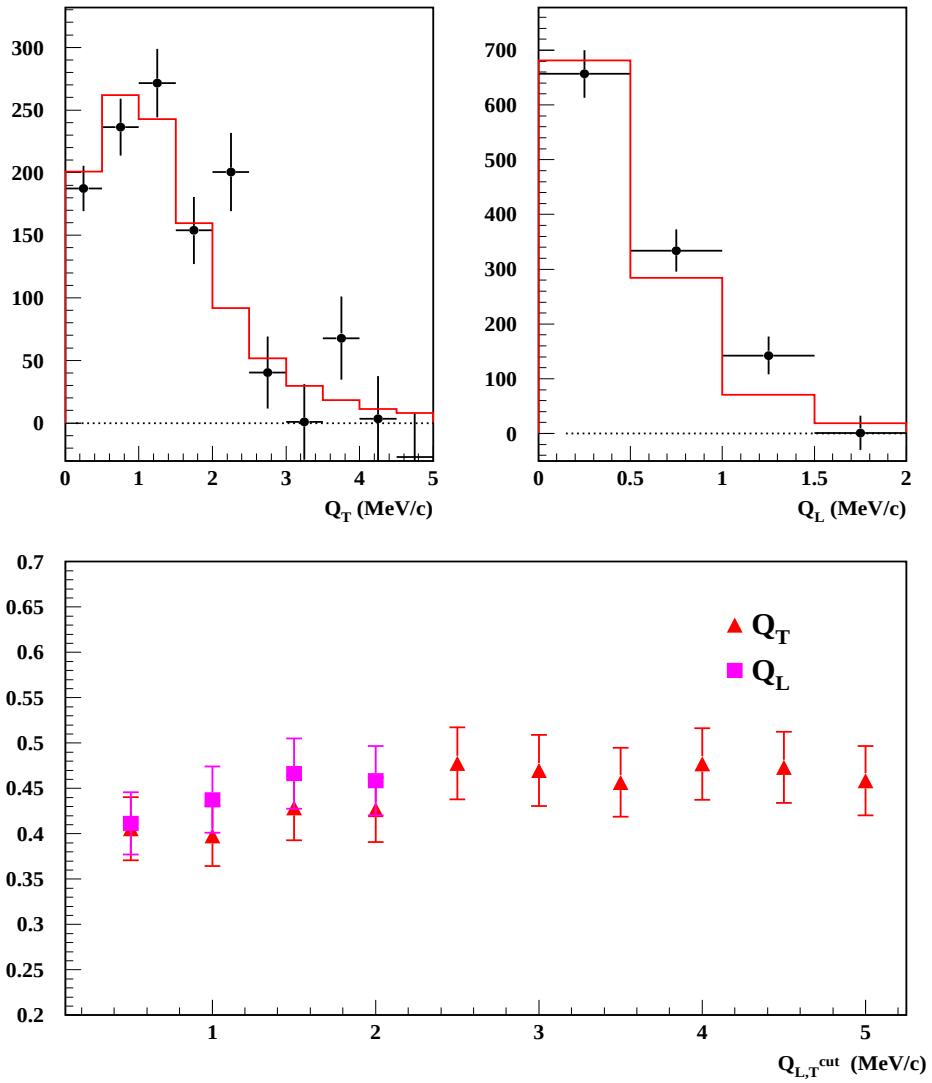

Fig. 10. *Fit results for a $\pi^+\pi^-$ momentum interval $4.4 < p < 5.0$ GeV/c in lab-frame. Caption is identical to figure 7.*

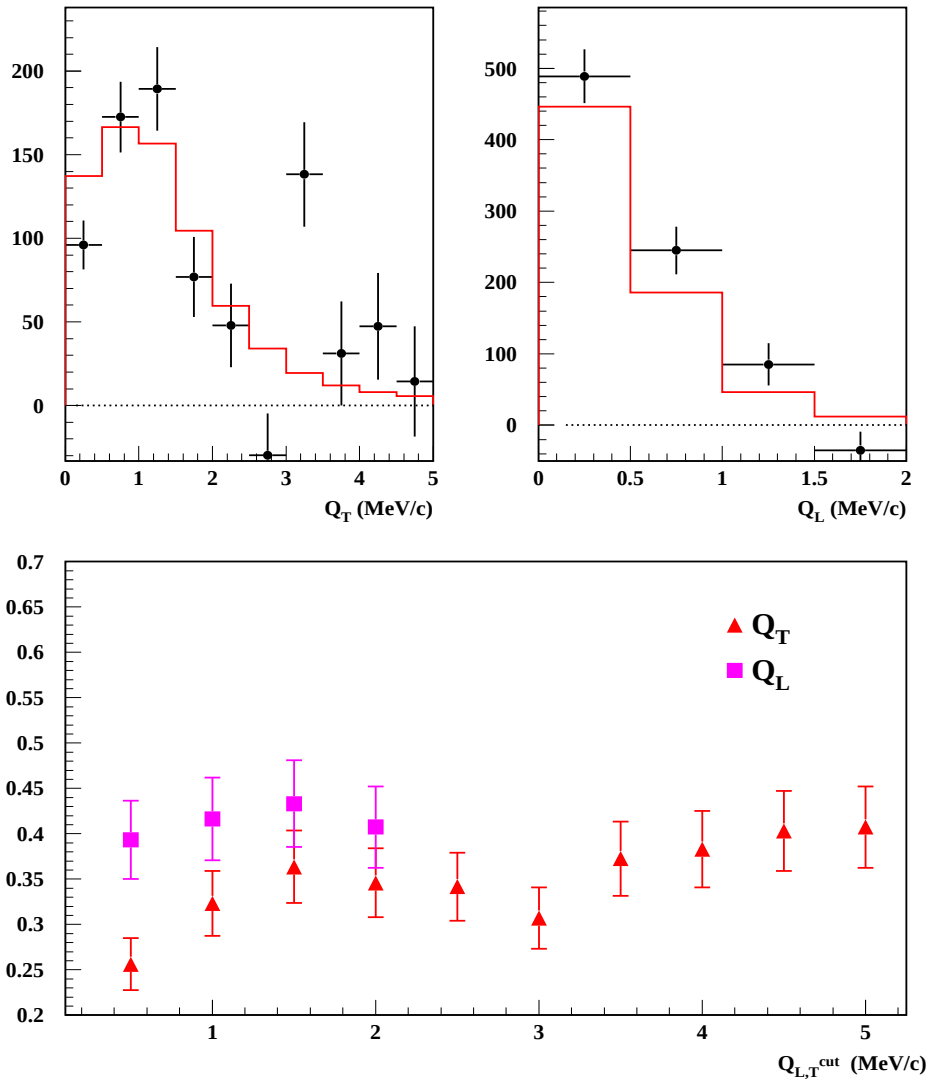

Fig. 11. *Fit results for a $\pi^+\pi^-$ momentum interval $5. < p < 5.6$ GeV/c in lab-frame. Caption is identical to figure 7.*

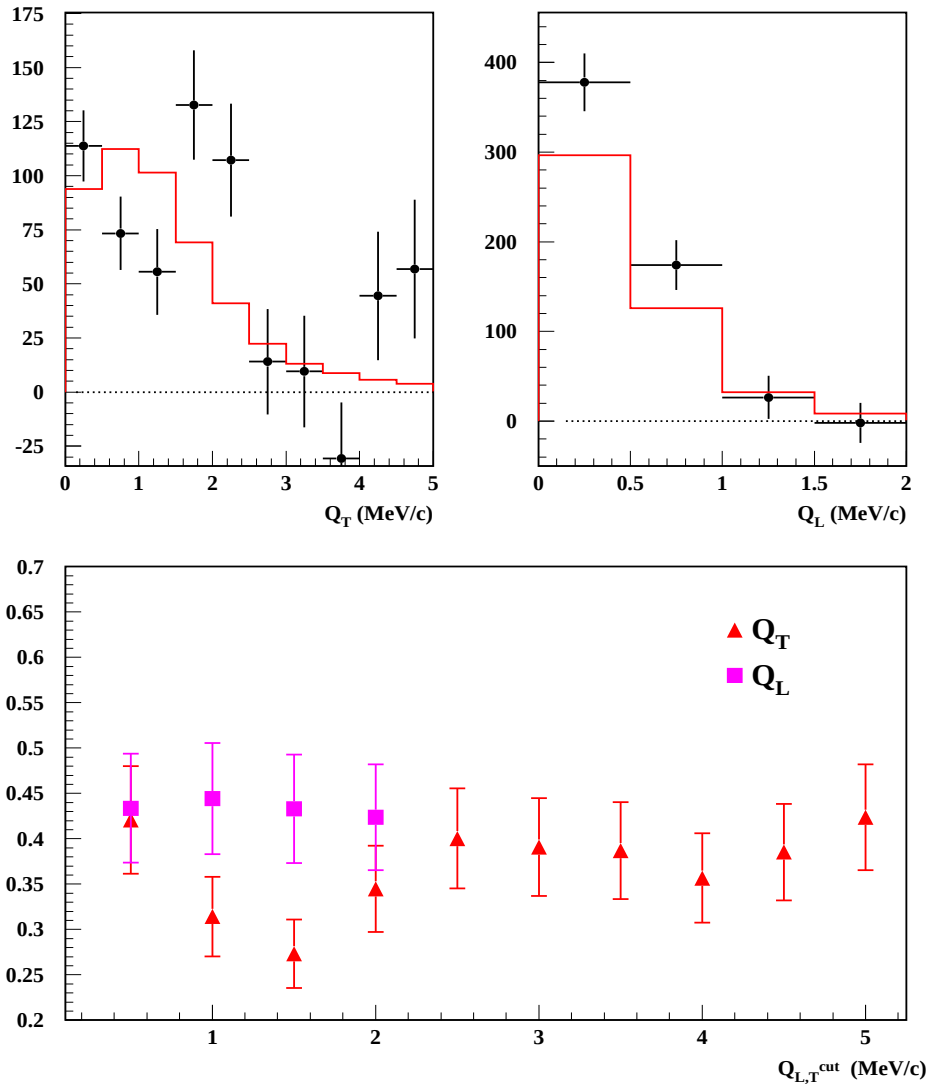

Fig. 12. *Fit results for a $\pi^+\pi^-$ momentum interval $5.6 < p < 6.2$ GeV/c in lab-frame. Caption is identical to figure 7.*

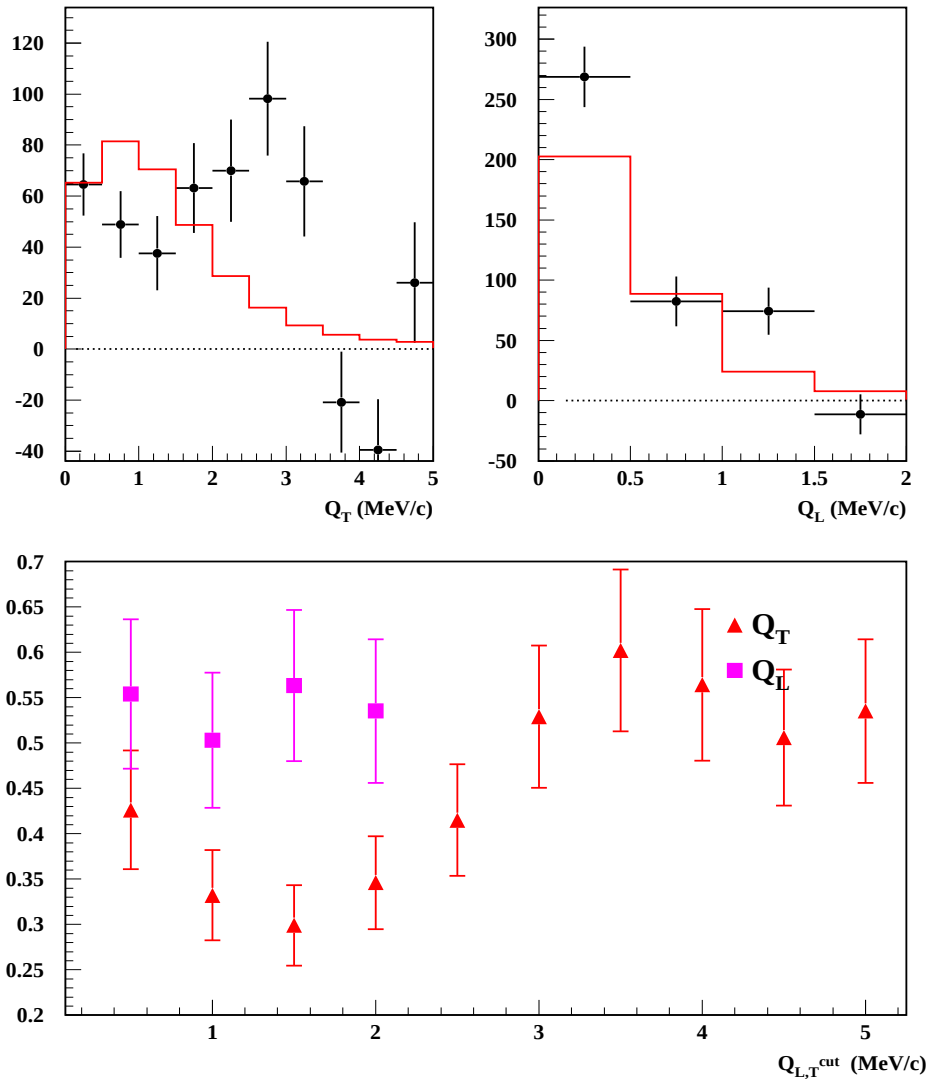

Fig. 13. *Fit results for a $\pi^+\pi^-$ momentum interval $6.2 < p < 6.8$ GeV/c in lab-frame. Caption is identical to figure 7.*

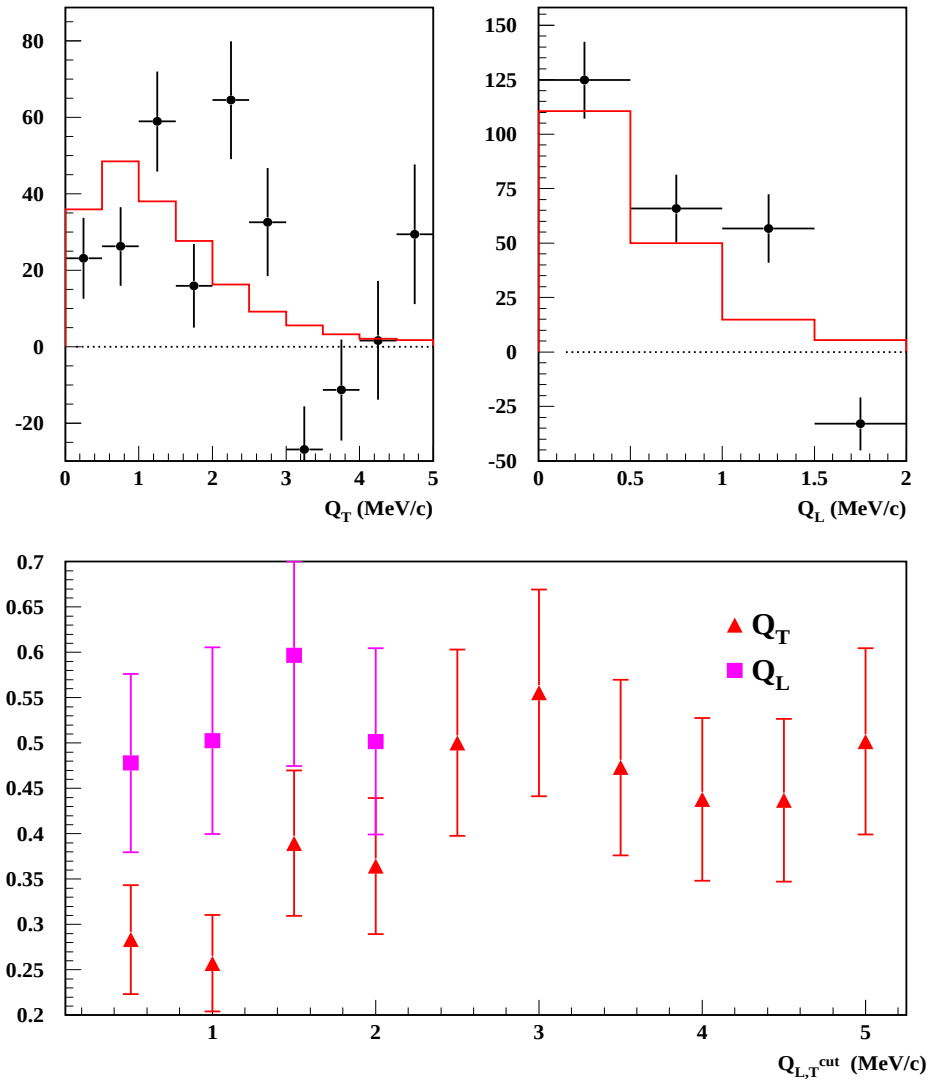

Fig. 14. *Fit results for a $\pi^+\pi^-$ momentum interval $6.8 < p < 7.4$ GeV/c in lab-frame. Caption is identical to figure 7.*

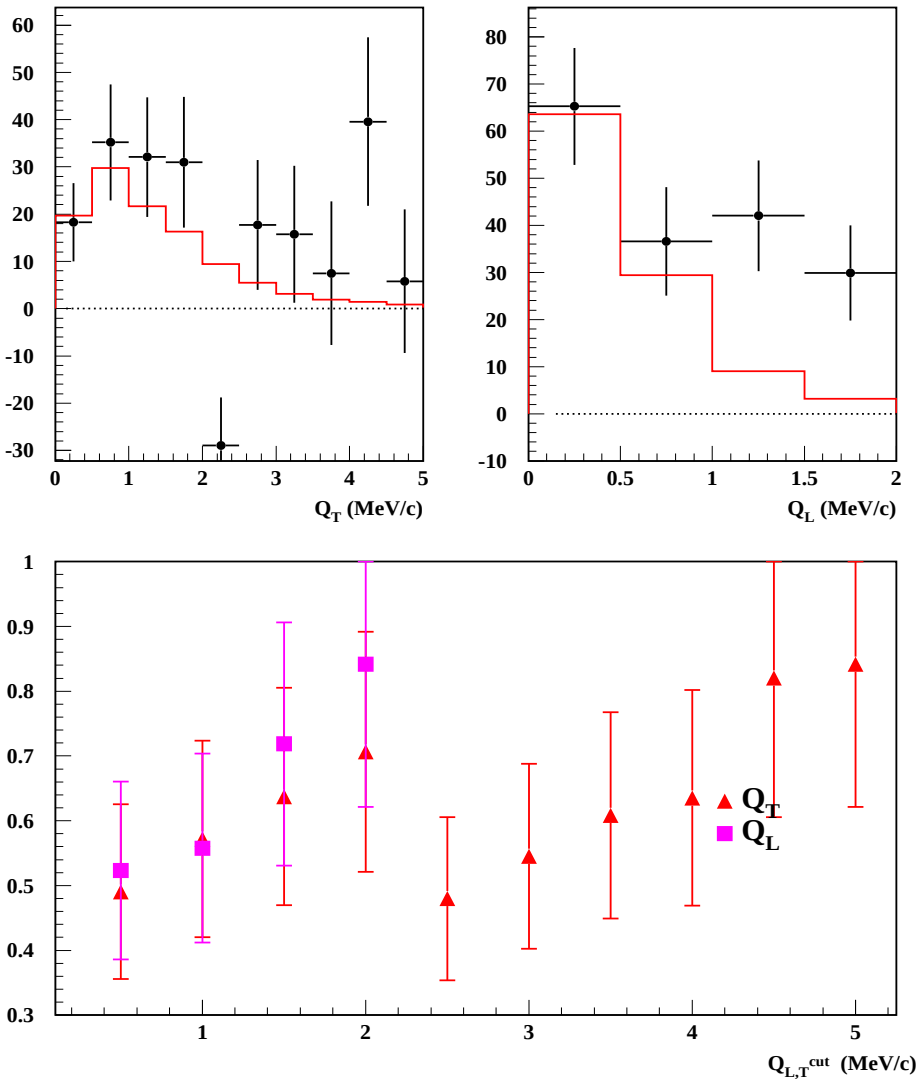

Fig. 15. *Fit results for a $\pi^+\pi^-$ momentum interval 7.4 $<$ p $<$ 8.0 GeV/c in lab-frame. Caption is identical to figure 7.*

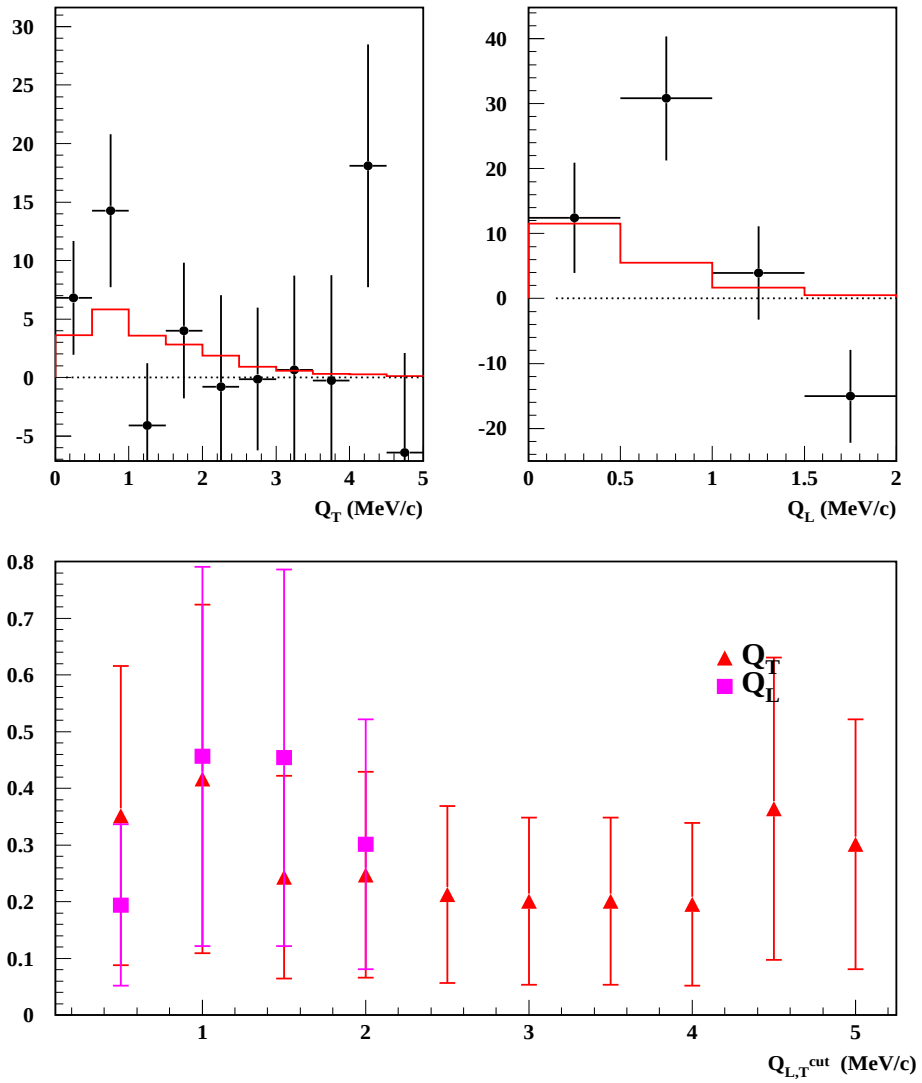

Fig. 16. *Fit results for a $\pi^+\pi^-$ momentum interval 8.0 $<$ p $<$ 8.6 GeV/c in lab-frame. Caption is identical to figure 7.*

8 Global fit results

In addition to the previous (momentum-dependent) analysis, we have also performed a global fit to the data, in which single parameters α, β and γ are left free to minimize the χ^2 defined in the momentum-integrated (Q_T, Q_L) plane by expression (1), summed over 0.25×0.25 $(MeV/c)^2$ bins. The fit results (case A) are indicated in table 6. Certainly the procedure allows a determination of a total number of atom pairs $\bar{N}_A$ and a mean break-up probability $\bar{P}_{Br}$ after taking into account the momentum-averaged K-factors.

These results are compared in table 6 with those obtained for N_A and P_{Br} by explicit sum and statistical averaging of the 10 values at individual momentum bins, respectively. χ^2-values and numbers of degrees of freedom have also been summed in these case (B). Their restriction to the control and extrapolation regions separately are shown in table 7. Fit results seem to be rather close, although we believe the momentum-dependent fit in narrow bins is more rigorous in view of possible acceptance correlations [13].

For visualization of the global atom signal projections, both methods provide nearly identical results. We show in figure 17 the Q_T spectrum, with the atom signal obtained by subtraction of Monte Carlo with pionium component removed. The prompt data are shown separately for the region $Q_L < 2MeV/c$ and $Q_L > 2MeV/c$. The longitudinal spectrum is shown in 18, and the relative momentum magnitude Q in figure 19. A 2D lego plot of the atom signal is shown in figures 20 and 21, where in the latter a signed transverse component Q_{xy} has been defined by projecting the measured value of Q_T over a randomly selected azimuth ϕ ($Q_{xy} = Q_T cos\phi$). As in previous section, P_{Br} values are shown as function of integration limits in Q_T and Q_L, now in $0.25MeV/c$ bins (see figure 23).

Provided there is good agreement between Monte Carlo and prompt data in Q_L projection, the measured values of the P_{Br} should not depend on the upper limit Q_L^c chosen for the fit. This is indeed the case, as it is illustrated in figure 22. We have safely chosen $Q_L^c = 20MeV/c$ for reference, in view of the fact that statistical errors from the fit are not improved anymore beyond this limit. The same situation is encountered at each individual momentum bin.

The fit procedure implies a correlation between α_1 and γ (proportional to N_A) which is displayed in figure 24 for the global fit. This correlation is taken into account in the statistical errors given in every momentum bin.

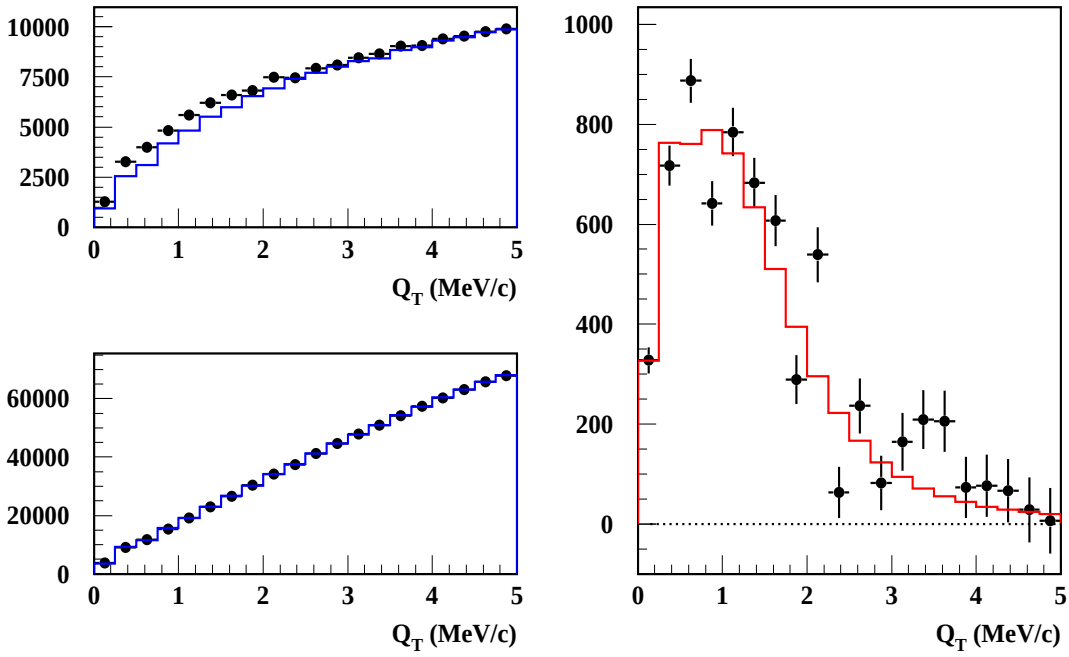

Fig. 17. *Two-dimensional fit projection onto Q_T. The data are shown separately for $Q_L < 2MeV/c$ and $Q_L > 2MeV/c$ (left plots). Non-Coulomb background is also shown as dotted line, after subtraction of 8.5 % accidentals . The difference between prompt data (dots) and Monte Carlo (blue line), which corresponds to transverse pionium signal, is plotted (right) and compared with the pionium atom Monte Carlo (red line).*

Table 6
Comparison of fit results with α_1 and γ as global fit parameters (A) and superposition of 10 independent fits at different 600 MeV/c momentum bins (B).

	χ^2 / ndf	α_2	P_{Br}	N_A	N_C
A	1516.7 / 1600	0.815 ± 0.006	0.438 ± 0.016	6738 ± 190	120611 ± 812
B	3853.2 / 3900	0.823 ± 0.015	0.432 ± 0.016	6761 ± 244	121323 ± 821

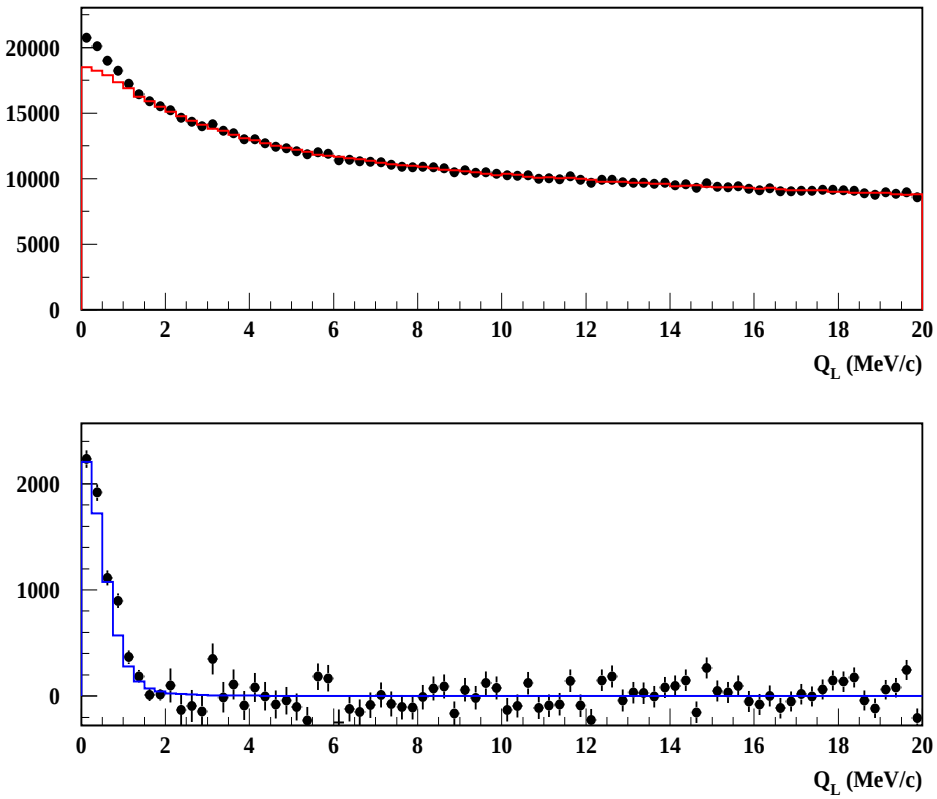

Fig. 18. *Two-dimensional fit projection onto Q_L. Non-Coulomb background, after subtraction of 8.5 % accidental pairs, is shown as dotted line. The difference between prompt data (dots) and Monte Carlo (blue line) , which corresponds to pionium signal, is plotted at the bottom, where the signal is compared with the pionium atom Monte Carlo (red line).*

Table 7
Comparison of the χ^2-values in the extrapolation ($Q_L < 2MeV/c$) and control ($Q_L > 2MeV/c$) regions for the fits A and B indicated in table 6.

	χ^2_e / ndf	χ^2_c / ndf
A	147.7 / 160	1368.9 / 1440
B	428.7 / 400	3424.4 / 3500

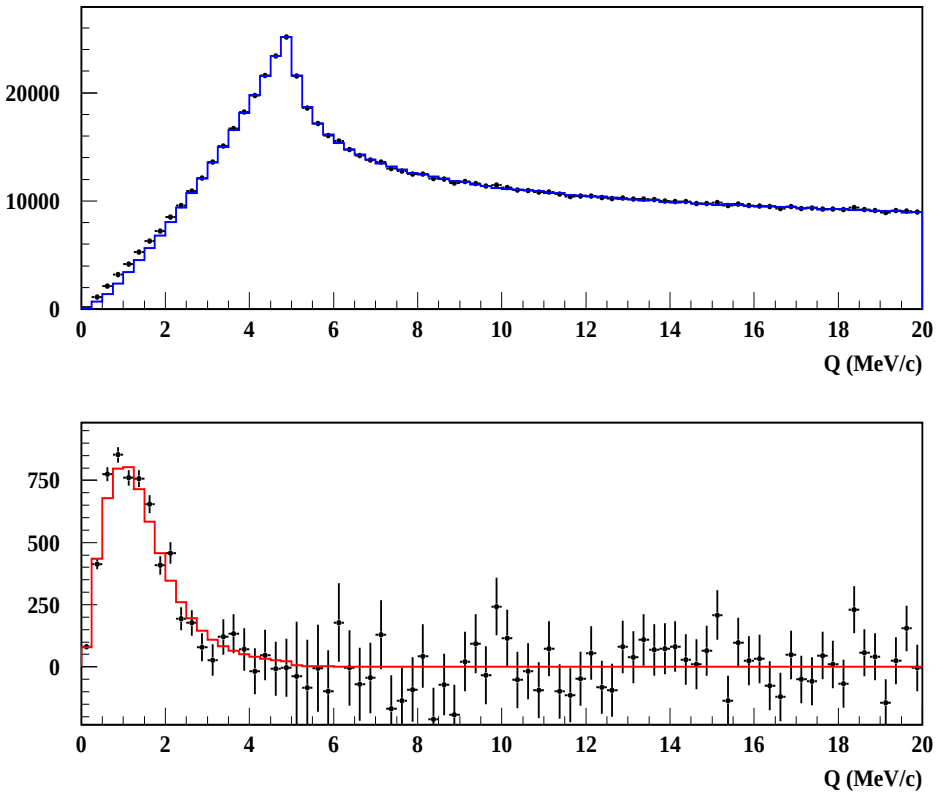

Fig. 19. *Two-dimensional fit projection onto Q. Non-Coulomb background, after subtraction of 8.5% accidentals, is shown as dotted line. The difference between prompt data (dots) and Monte Carlo (blue line) , which corresponds to pionium signal, is plotted at the bottom. The signal is compared with the pionium atom Monte Carlo (red line).*

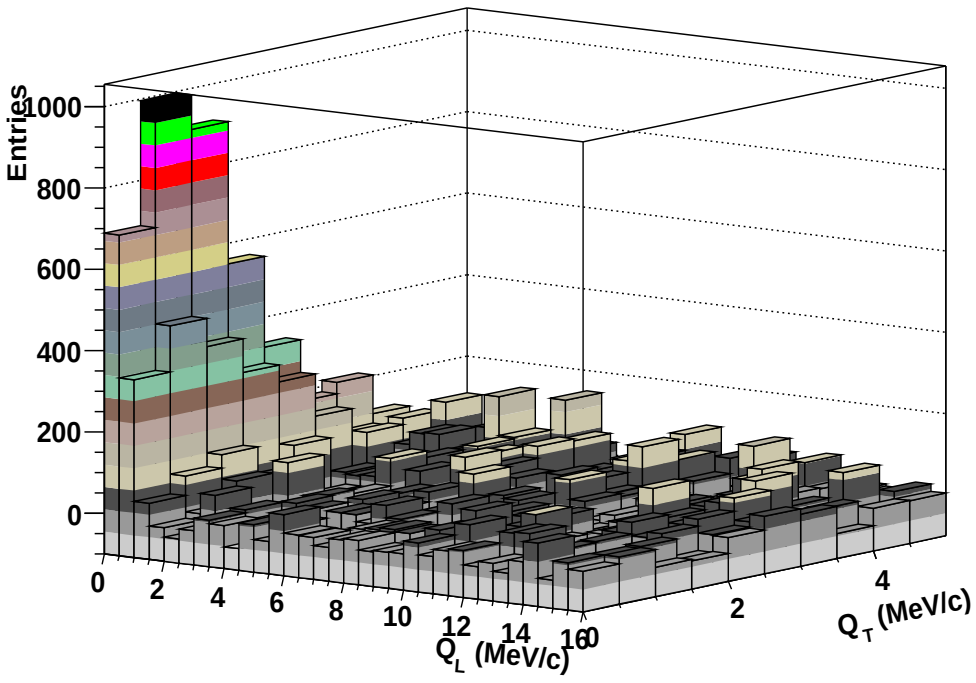

Fig. 20. *Lego plot showing pionium break-up in* $(Q_T, Q_L = |Q_Z|)$ *plane*

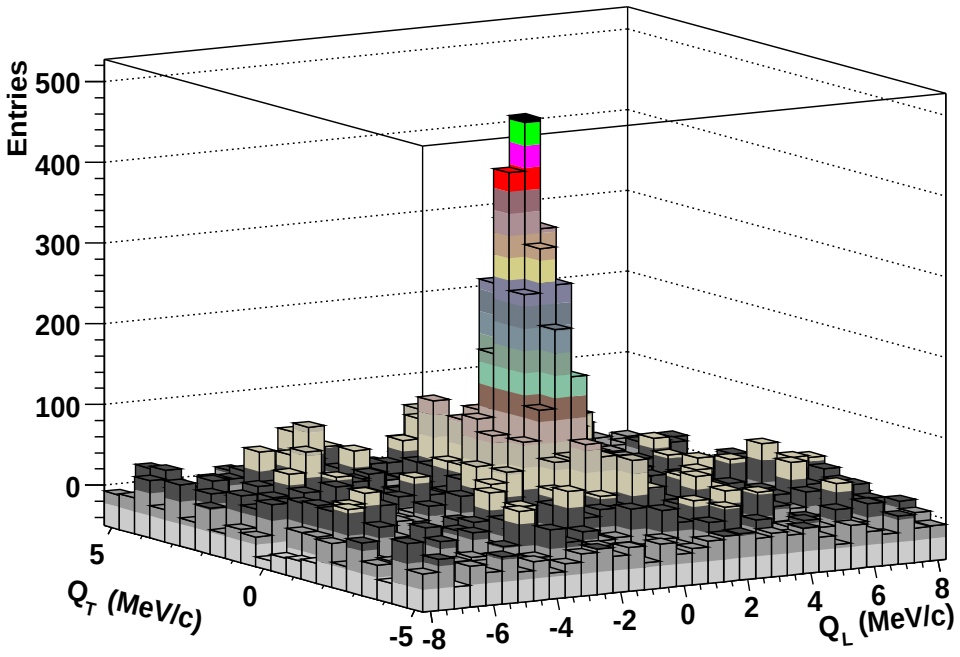

Fig. 21. *Lego plot showing pionium break-up in* (Q_{xy}, Q_L) *plane. The transverse component* $Q_{xy} = Q_T\ cos\phi$ *is defined as the product of the measured* Q_T *value times the cosine of a random azimuth.*

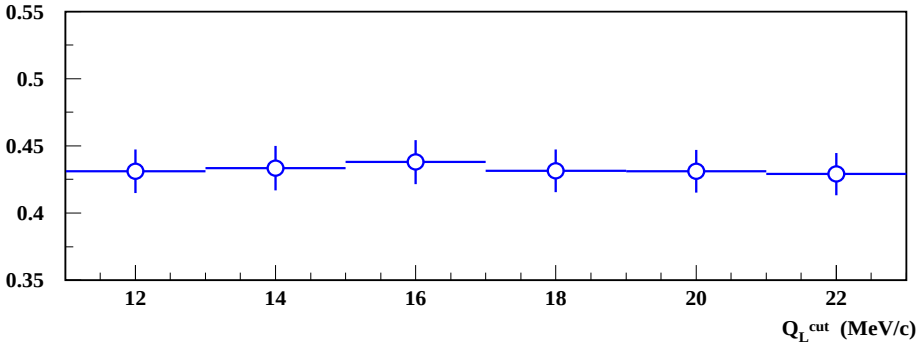

Fig. 22. *Measured values of* P_{Br} *as function of* Q_L *upper limit in the fit* (Q_L^c) .

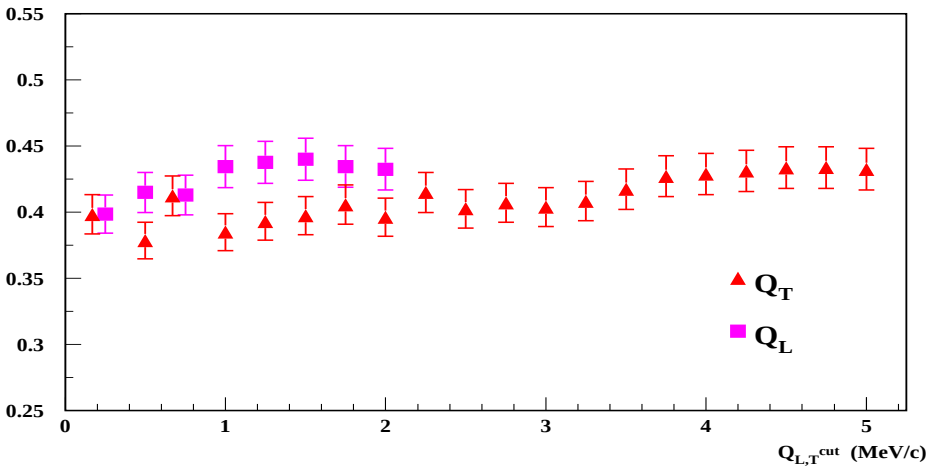

Fig. 23. *Measured break-up probability as function of Q_L and Q_T cuts.*

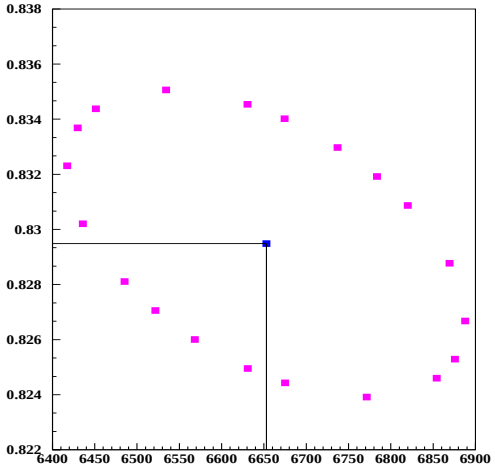

Fig. 24. *1σ contour plot calculated by MINOS program for α_1 and the number of atoms N_A found by the global 2D-fit, showing statistical errors and correlation.*

9 Systematic error

We have studied the magnitude and sign of possible systematic errors in the measurement of break-up probability P_{Br}, related to imperfect simulation of detector response and to other effects. The most significant contributions we found are the following:

- knowledge of average multiple scattering angle in upstream detectors
- correction for non-uniformity of Q_L trigger acceptance
- simulation of MSGC background
- simulation of pionium atom signal
- simulation of Q_T spectrum
- finite-size effects and η' / ω contamination

The total radiation length of upstream detectors is known with $\pm 1.5\%$ precision and has been the subject of a detailed study [9]. Furthermore, its contribution to Q_T resolution is much reduced by the exclusive utilization of MSGC/GEM signals in the final track fitting [5]. Note that the X and Y planes (located closest to the target foil) are essentially free of multiple scattering in the spectrometer. A $\pm 1.5\%$ variation of the average θ_{MS} angle produces a negligible change in the Monte Carlo spectrum of pionium. A maximum uncertainty of $\Delta P_{Br} = \pm 0.003$ is attributed to this particular source.

Results have shown that the Q_L trigger acceptance correction determined from accidental pairs works well in describing correctly the Coulomb spectrum. Having used the full sample of accidental pairs for Ni 2001, we are probably still limited by statistics (specially at large momentum) for a precision knowledge of this correction, and there we find one source of systematic error. From variations of the correction structure, compatible with the accidentals pattern, we estimate $\Delta P_{Br} = \pm 0.007$ as a maximum possible shift of P_{Br}.

MSGC background has also been the subject of very detailed study [5] [9]. The probability of noise hits entering the real tracks is known very precisely, as figure 1 shows. We assign a maximum systematic error to this concept of $\Delta P_{Br} = \pm 0.006$.

Momentum resolution of the spectrometer was determined rather accurately using small Q_T Λ pairs and the Monte Carlo simulation was cross-checked according to it [18]. We think this work is behind the good agreement between the pionium Monte Carlo and the experimental signal in figure 18. We assign a very small error to the fact that we use this Monte Carlo to guide the 2D fit, since the hypothesis is well consistent with the data.

Simulation of SFD signals (including PSC) and background has been optimized according to the work in [15], and it has little influence on the final Q_T

spectrum. SFD inefficiency, on the other hand, has been accurately determined by means of MSGC/GEM detector [14]. It contributes to the observed rate of single-track events [5], but the analysis of the Q_T spectrum in the region $Q_L > 2MeV/c$ provides a good handle to reduce this particular simulation uncertainty. We assign a global ± 0.003 maximum systematic error coming from imperfect simulation of the Q_T spectrum, and double-track resolution.

Finally, we have incorporated to our analysis a correction to the P_{Br} measurement originated from the effect of large-size resonances η' and ω, as well as finite-size nuclear effects [6] on the Coulomb spectrum. This correction is based on a 1% η' and 19% ω contamination, determined by with the UrQMD Monte Carlo, and on parametrizations of nuclear size, cross-checked with real $\pi^+\pi^+$ data from the spectrometer [16]. The systematic error we associate with this correction comes from a $\pm 25\%$ uncertainty in the production of ω resonance, which is the dominant effect.

Without knowledge of correlations between the above sources of systematic error, we have convoluted them by generating random numbers with squared-pulse shape probability distributions, the width being determined by the contents of the second column in table 8. A gaussian fit to the resulting distribution provides a 1σ equivalent to the combined systematic error of ± 0.009 wich can be added in quadrature to the statistical error, for the sake of synthesis. The resulting P_{br} measurement is then 0.432 ± 0.016 (stat) $\pm$ 0.009 (syst) = 0.432 ± 0.018.

Table 8

Estimated contributions to systematic error in average break-up probability measurement. Last row indicates total systematic error equivalent to 1σ, under the assumption of uncorrelated effects.

Simulation error	ΔP_{Br} extreme values
Multiple scattering ($\pm 1.5\%$)	± 0.003
Q_L trigger acceptance	± 0.007
MSGC background	± 0.006
Atom signal shape	± 0.002
Double-track resolution	± 0.003
Finite-size correction ($\pm 25\%$ ω)	± 0.003
Total 1σ equivalent	± 0.009

10 Summary and conclusions

Without consideration of any finite-size correction, the $1s$ lifetime of pionium atom has been determined to be:

$\tau_{1S} = 2.64^{+0.32}_{-0.18}(stat)$

following the analysis of previous sections. When the finite-size correction $\Delta P_{Br} = -0.009 \pm\ 0.003$ is taken into account, the result becomes :

$$\tau_{1S} = 2.58^{+0.26}_{-0.22}(stat)^{+0.15}_{-0.14}(syst)$$

A quadrature of both sources of error yields the combined result :

$$\tau_{1S} = 2.58^{+0.30}_{-0.26}$$

which can be converted into a measurement of the s-wave amplitude difference:

$$|a_1 - a_0| = 0.280\ ^{+\ 0.016}_{-\ 0.014}\ M_\pi = (0.280 \pm 0.015)\ M_\pi$$

by means of the expression [19]:

$$\Gamma_{1s} = \frac{1}{\tau_{1s}} = \frac{2}{9}\alpha^3 p\ |a_1 - a_0|^2 (1+\delta)\ M_\pi^{-2}$$

where $\delta = (5.8 \pm 1.2) \times 10^{-2}$ and $p = \sqrt{M_{\pi+}^2 - M_{\pi 0}^2 - (1/4)\alpha^2 M_{\pi+}^2}$.

11 Acknowledgements

This work would not have been possible without the strong support of Centro de Supercomputación de Galicia (CESGA), which we would like to thank here institutionally. The technical help received from J.J. Saborido Silva and M. Sánchez Garcia, who facilitated us the use of this strong computing network at USC, is also warmly appreciated. Our gratitude is extensive to Carlos Fernández Sánchez, in charge of the SVGD cluster at CESGA. We also thank Cibrán Santamarina Rios for useful comments, advice and technical help concerning pionium simulation.

References

[1] B. Adeva et al. DIRAC : A High Resolution Spectrometer for Pionium Detection, Nucl. Inst. and Meth. A515 (2003) 467-496.

[2] DIRAC note 98-08. The GEANT-DIRAC Simulation Program Version 2.5. P. Zrelov and V. Yazkov.
http://zrelov.home.cern.ch/zrelov/dirac/montecarlo/instruction/instruct26.html

[3] The DIRAC offline User Guide. Daniel Drijard, Michel Hansroul and Valery Yazkov.

[4] DIRAC note 03-08: A Tracking System for Upstream Detectors in DIRAC, B. Adeva, A. Romero and O. Vázquez Doce.

[5] DIRAC Note 05-15: Full-Tracking Resolution in DIRAC with 2001 Data, B. Adeva, A. Romero and O. Vázquez Doce.
DIRAC Note 05-19: Addendum to Full-Tracking Resolution in DIRAC with 2001 Data, B. Adeva, A. Romero and O. Vázquez Doce.

[6] DIRAC note 04-06: Finite-size effects on two-particle production in continuous and discrete spectrum, R. Lednicky .

[7] DIRAC note 04-02: DIRAC events generator, C. Santamarina.

[8] DIRAC Note 02-10: Proton to pion ratio in accidental coincidences, S. Trusov.

[9] DIRAC Note 05-16: Study of Multiple Scattering in Upstream Detectors in DIRAC, B. Adeva, A. Romero and O. Vázquez Doce.

[10] C. Santamaria, M. Schuman, L.G. Afanasyev, T. Heim, A Monte-Carlo Calculation of the Pionium Breakup Probability with Different Sets of Pionium Target Cross Sections, J. Phys. B. At. Mol. Opt. Phys. 36 4273 (2003), arXiv:physics/0306161 v1.

[11] DIRAC note 03-09: Determination of the experimental k-factor, C. Santamarina and C. P. Schutz.

[12] L. Afanasyev, Observation of $\pi^+\pi^-$ atoms, Ph. D. Thesis, JINR, Dubna (1997). Afanasyev L G et al. Phys. At. Nucl. 60 938 (1997).

L.G. Afanasyev. O.O. Voskressenskaya, V.V.Yazkov, Communication JINR P1-97-306, Dubna, 1997.

[13] L. Afanasyev et al., Measurement of a Coulomb Interaction Effect in $\pi^+\pi^-$ pairs from the Reaction $pTa \to \pi^+\pi^-$ at 70 GeV, Physics of Atomic Nuclei, Vol. 60, No. 6, 938 (1997)

[14] DIRAC Note 05-11: Study of SFD Efficiency Using MSGC Detector for 2001 Data, B. Adeva, A. Romero and O. Vázquez Doce.

[15] DIRAC Note 05-04: Experimental and simulated response of ScFi detector, V. V. Yazkov.

[16] "Measurement of pionium lifetime and study of correlation of particles with relative small velocities", J. Smolik. Doctoral Thesis, Faculty of Physics and Mathematics Charles University, Prage, August 2005.

[17] DIRAC note 05-01: Dependence of break-up probability estimation on K^+K^- and $p\bar{p}$ background, O. Gortchakov and V.V. Yazkov .

[18] DIRAC note 04-06 : Experimental determination of momentum resolution in DIRAC using Lambda events, B. Adeva, A. Romero and O. Vázquez Doce.

[19] J. Gasser et al., Phys. Rev. D 64 (2001) 016008, hep-ph/0103157.